

¹ **Estimating χ and K_T from fast-reponse thermistors on traditional shipboard**

² **CTDs: sources of uncertainty and bias.**

³ Andy Pickering*

⁴ *College of Earth, Ocean, and Atmospheric Sciences, Oregon State University, Corvallis, OR.*

⁵ Jonathan Nash

⁶ *College of Earth, Ocean, and Atmospheric Sciences, Oregon State University, Corvallis, OR.*

⁷ Jim Moum

⁸ *College of Earth, Ocean, and Atmospheric Sciences, Oregon State University, Corvallis, OR.*

⁹ Jen MacKinnon

¹⁰ *UCSD / Scripps Institute of Oceanography*

¹¹ *Corresponding author address: College of Earth, Ocean, and Atmospheric Sciences, Oregon State University, Corvallis, OR.

¹³ E-mail:

ABSTRACT

14 The acquisition of turbulence data from traditional shipboard CTD casts is
15 attractive for its potential to dramatically increase the amount of deep-ocean
16 mixing observations globally. While data from shear-probes are easily con-
17 taminated by motion of the instrument platform, the measurement of tempera-
18 ture gradient is relatively insensitive to vehicle vibration, making it possible to
19 measure temperature gradient from a shipboard CTD rosette. The purpose of
20 this note is to investigate and quantify the error and bias in estimating the rate
21 of dissipation of temperature variance χ and turbulent diffusivity K_T acquired
22 during traditional CTD profiling. The most significant source of error is as-
23 sociated with the fact that fast-response FP07 thermistors resolve only a frac-
24 tion of the temperature gradient variance at the fallspeed of typical CTD casts.
25 Assumptions must be made about the wavenumber extent of the temperature
26 gradient spectrum, which scales with the rate of dissipation of turbulent kinetic
27 energy, a quantity that is not directly measured. Here we utilize observations
28 from a microstructure profiler to demonstrate the validity of the method of es-
29 timating χ from thermistor data, and to assess uncertainty and bias. We then
30 apply this methodology to temperature gradient profiles obtained from χ pods
31 mounted on a CTD (the CTD- χ -pod), and compare these to microstructure
32 profiles obtained almost synoptically at the equator. CTD- χ -pod estimates of
33 χ compare favorably to the direct microstructure measurements and demon-
34 strate that the χ -pod method is not significantly biased. This supports the
35 utility of the measurement as part of the global repeat hydrography program
36 cruises, during which this type of data has been acquired during the past few
37 years.

³⁸ **1. Introduction**

³⁹ Turbulent mixing affects the distribution of heat, salt, and nutrients throughout the global ocean.

⁴⁰ Diapycnal mixing of cold, dense water with warmer water above maintains the abyssal overturning

⁴¹ circulation (Munk 1966; Munk and Wunsch 1998), which affects global climate. Because the

⁴² turbulence that drives mixing generally occurs at scales that are not resolved in climate models,

⁴³ it must be parameterized, based on either (i) aspects of the resolved model dynamics, (ii) through

⁴⁴ higher resolution models that capture the dynamics that feed energy to turbulence, or (iii) using

⁴⁵ other parameterizations that either dynamically or statistically quantify turbulent fluxes. Recent

⁴⁶ investigations have demonstrated that these models are sensitive to the magnitude and distribution

⁴⁷ of mixing (Melet et al. 2013). A comprehensive set of measurements that spans relevant dynamical

⁴⁸ regimes is needed to constrain mixing and develop more accurate parameterizations.

⁴⁹ Direct measurement of mixing with microstructure profilers equipped with shear probes is ex-

⁵⁰ pensive, time-intensive, and requires considerable care and expertise. Moreover, tethered profilers

⁵¹ can't reach abyssal depths, requiring autonomous instruments to get deeper than \sim 1000-2000 m.

⁵² As a result, existing measurements of diapycnal mixing, especially in the deep ocean, are sparse

⁵³ (Waterhouse et al. 2014). In order to obtain estimates over a larger area, considerable work has

⁵⁴ gone into inferring mixing from measurements of the outer scales of turbulence, which are easier

⁵⁵ to obtain. One popular method is the use of Thorpe scales, where diapycnal mixing is inferred

⁵⁶ from inversions in profiles of temperature or density (Thorpe 1977; Dillon 1982). The size of

⁵⁷ resolvable overturn is limited by the profiling speed and instrument noise (Galbraith and Kelley

⁵⁸ 1996). Several studies indicate relatively good agreement with microstructure and other observa-

⁵⁹ tions, but there are some questions about the validity of the method and the assumptions made

⁶⁰ (Mater et al. 2015; Scotti 2015). Parameterizations based on profiles of shear and/or strain have

also been developed and applied to estimate diapycnal mixing (Gregg 1989; Kunze et al. 2006; Polzin et al. 2013; Whalen et al. 2012, 2015). However, they rely on a series of assumptions about the cascade of energy from large to small scales that are often violated; numerous studies (i.e., Waterman et al. (2013) have shown that there is significant uncertainty associated with these parameterizations, in that there can be a consistent bias in a particular region, yet the sense of the bias (i.e., overpredict vs. underpredict) is not known *a priori*.

Quantifying turbulence from velocity shear variance (to compute the dissipation rate of turbulent kinetic energy ε) is challenging on moorings or profiling platforms because there is usually too much vibration and/or package motion for shear-probes to be useful. Other methods (i.e., optics or acoustics) may hold some promise, but lack of scatterers often precludes this type of measurement, especially in the abyss. In addition, shear probes only provide ε , not the mixing of scalars, K , which is often inferred from ε by assuming a mixing efficiency Γ (Osborn 1980) as $K = \Gamma \varepsilon / N^2$, which N^2 is the buoyancy frequency. A more direct measure of the turbulent mixing is obtained from the dissipation rate of temperature variance χ (Osborn and Cox 1972). This has the advantage that (i) temperature and temperature gradient is relatively straightforawrd to measure, and (ii) the estimation of mixing from χ does not rewuire assumptions about Γ . However, the spectrum of temperature gradient extends to very small scales, so that its spectrum is seldom fully resolved (and unlike shear variance, the wavenumber extent of the spectrum is not related to the amplitude of the temperature (or temperature gradient) spectrum). Assumptions about the spectral shape (Kraichnan vs. Bachelor, and the value of the “constant” q) and its wavenumber extent (governed by the Batchelor wavenumber $k_b = [\varepsilon / (v D_T^2)]^{1/4}$ (Batchelor 1959)) are thus necessary to determine χ unless measurements capture the full viscous-diffusive subrange of turbulence (i.e., down to scales $\Delta x \sim 1/k_b \sim 1\text{mm}$), a criterion seldom achieved. To resolve this, we follow Alford and

⁸⁴ Pinkel (2000) and Moum and Nash (2009) and make the assumption that $K_T = K_\rho$ to determine
⁸⁵ the dissipation rate as $\varepsilon_\chi = (N^2 \chi) / (2\Gamma \langle dT/dz \rangle^2)$, permitting k_b to be estimated.

⁸⁶ The goal of this paper is to outline and validate the methods used to compute χ and K_T with
⁸⁷ χ -pods mounted on CTDs. We do this by applying our processing methodology to profiles of tem-
⁸⁸ perature gradient measured by thermistors on the ‘Chameleon’ microstructure profiler, which pro-
⁸⁹ vides a direct test of our methodology. Because Chameleon is a loosely tethered profiler equipped
⁹⁰ with shear probes (Moum et al 1995), it directly measures ε and allows us to test our assumptions.
⁹¹ Specifically, it allows us to determine biases associated with computing chi from partially-resolved
⁹² temperature alone, as compared to that when it is computed by including knowledge of the dissi-
⁹³ pation rate, which constrains the wavenumber extent of the scalar spectra. After establishing that
⁹⁴ the method works, we then compare CTD- χ pod profiles to nearby microstructure profiles.

⁹⁵ 2. Data

⁹⁶ a. EQ14

⁹⁷ Data were collected on the R/V Oceanus in Fall 2014 during the EQ14 experiment to study
⁹⁸ equatorial mixing. More than 2700 Chameleon profiles were made, along with 35 CTD-chipod
⁹⁹ profiles bracketed by chameleon profiles in order to maintain calibrations during the cruise. Most
¹⁰⁰ Chameleon profiles were made to depth of about 250m, with CTD casts going to 500m or deeper.
¹⁰¹ The EQ14 experiment and results are discussed in more detail in (Buoyant gravity currents re-
¹⁰² leased from tropical instability waves, JPO (SJ Warner, RN Holmes, EH McHugh-Hawkins, JN
¹⁰³ Moum) , in preparation).

104 **3. Methods**

105 As mentioned in the introduction, the temperature gradient spectrum is rarely fully resolved
106 down to the small scales of turbulent mixing. The fraction of the spectrum resolved depends on
107 the true spectrum (a function of χ and ε), the flowspeed past the sensor ('fspd'), and the response
108 of the thermistor. The GE/Thermometrics FP07 thermistors we use typically resolve frequencies
109 up to about 10-15 Hz (??). The maximum resolved wavenumber is then equal to $k_{max} = f_{max}/u$,
110 while the wavenumber extent of the true spectrum varies with kb (and the quarter power of ε).
111 At the typical vertical fall rate of a CTD rosette ($\sim 1\text{m/s}$), only about 20% of k_b is resolved at
112 $\varepsilon = 10^{-9}$ (Figure 2). While methods have been developed to fit the observed temperature gradient
113 spectrum to theoretical forms (Ruddick et al. 2000), these work only when a large fraction of the
114 temperature gradient spectrum is resolved. For the relatively high profiling speeds typical of CTD
115 casts, we find these methods do not work well (see appendix for details) and therefore we use a
116 different method.

117 We first outline our method for estimating χ , which relies on (i) determining the instantaneous
118 flowspeed past the sensor, (ii) identifying periods where the signals may be contaminated by the
119 wake of the CTD rosette, (iii) defining the relavent N^2 and $(dT/dz)^2$, and (iv) JN: WHAT ELSE?...
120 We then discuss some limitations and practical considerations that arise.

121 *a. Iterative Method for estimating χ*

122 For each ~ 1 second window, χ is estimated via the following procedure as outlined in Moum
123 and Nash (2009). For isotropic turbulence,

$$\chi_T = 6D_T \int_0 \Psi_{T_x}(k) dk \quad (1)$$

124 where D_T is the thermal diffusivity and $\Psi_{T_x}(k)$ is the wavenumber spectrum of dT/dx .

125 Note that dT/dx is not measured; dT/dt is measured, and dT/dx is inferred from Taylor's
 126 frozen flow hypothesis

$$\frac{dT}{dx} = \frac{1}{u} \frac{dT}{dt} \quad (2)$$

127 The wavenumber extent of the spectrum depends on the Batchelor wavenumber k_b , which is
 128 related to ε :

$$k_b = [\varepsilon / (v D_T^2)]^{1/4} \quad (3)$$

129 We assume that $K_\rho = K_T$ and $K_\rho = \Gamma \varepsilon / N^2$. Then dissipation rate is computed as

$$\varepsilon_\chi = \frac{N^2 \chi_T}{2\Gamma \langle dT/dz \rangle^2} \quad (4)$$

130 Typical thermistors do not resolve the spectrum out to k_b , so the measured spectrum is fit to the
 131 Kraichnan form of theoretical scalar spectrum over the range of resolved wavenumbers ($k_{min} <$
 132 $k < k_{max}$). The variance between the measured $[\Phi_{T_x}(k)]_{obs}$ and theoretical $[\Phi_{T_x}(k)]_{theory}$ spectra at
 133 these wavenumbers is assumed to be equal:

$$\int_{k_{min}}^{k_{max}} [\Phi_{T_x}(k)]_{obs} dk = \int_{k_{min}}^{k_{max}} [\Phi_{T_x}(k)]_{theory} dk \quad (5)$$

134 JN: need to explicitly state how χ is computed (integral of spectrum...).... ???? (you state a
 135 formula for ε_χ but not χ)....

136 An iterative procedure is then used to fit and calculate χ and ε :

137 1. First we estimate χ_T based on an initial guess of $\varepsilon = 10^{-7}$ W/kg and compute k_b . We
 138 set $k_{max} = k_b/2$ or to a wavenumber equivalent to $f_{max} = 7$ Hz [i.e., $k_{max} = 2\pi(f_{max})/u$],
 139 whichever is smaller. We choose $f_{max} = 7$ Hz because the thermistors' response rolls off at
 140 higher frequencies (see appendix).

141 2. We then use Eq. (4) to refine our estimate of k_b and recompute χ_T using Eqs. (1) and (??).

¹⁴² 3. This sequence is repeated and converges after two or three iterations.

¹⁴³ Note that this procedure is equivalent to the explicit formulation of (Alford and Pinkel 2000),
¹⁴⁴ except we use the Kraichnan spectrum. *JN and then it isn't possible to have the closed form the M*
¹⁴⁵ *used - us this true? If it is, then state that, and if it isn't, then we should just solve for it...*

¹⁴⁶ b. *CTD-χpod Data Processing*

¹⁴⁷ The basic outline for processing each CTD- χ -pod profile is as follows:

¹⁴⁸ 1. The correct time-offset for the χ -pod clock is determined by aligning dp/dt from the 24Hz
¹⁴⁹ CTD data to vertical velocity calculated by integrating vertical accelerations measured by the
¹⁵⁰ χ -pod. χ -pod clock drift is small, typically on the order of 1 sec/week, but it is imperative to
¹⁵¹ get records aligned within < 0.5 s so that the correct $u = w = dp/dt$ is used.

¹⁵² 2. Low-order polnomical calibration coefficients are determined to convert thermistor voltages
¹⁵³ from χ pod to ITS90 temperature (as measured by the CTD. Figure 3 shows an example of
¹⁵⁴ the aligned and calibrated CTD- χ pod timeseries for one cast. Note the significant differences
¹⁵⁵ in amount of variance associated with the two sensors during down and up casts. For the
¹⁵⁶ upward-mounted sensor (T1), the downcast signal is entirely associated with the CTD wake,
¹⁵⁷ as is the upcast for the downward-mounted sensor (T2). Only the ‘clean’ portions of the cast
¹⁵⁸ (e.g., the T1 upcast and the T2 downcast) are used in the χ pod calculations.

¹⁵⁹ 3. Depth loops are identified and flagged in the 24Hz CTD data. χ -pod data during these times
¹⁶⁰ are discarded since the signals are likely contaminated by the wake of the CTD. Even for
¹⁶¹ profiles that are significantly affected by ship heaving, good segments of data are obtained
¹⁶² over a majority of the depths.

- 163 4. Buoyancy frequency N^2 and temperature gradient dT/dz are computed from 1-m binned CTD
164 data. JN: I still like the idea of including some P data... but perhaps see below...

165 5. Half-overlapping 1 sec windows of data are used to estimate χ , ε , and K_T following the
166 methods described in Moum and Nash (2009), outlined in the previous section.

167 c. *Example Spectra and Fits*

168 An example of the observed and fit spectra are shown in Figure 4. Although only a small portion
169 of the spectrum is used in the fit, the method gives good results for χ . Errors in ε tend to be larger,
170 due to additional assumptions required.

171 JN: would be good to have a few more details, comment on the location, quick review of how
172 the spectrum is fit, etc. Also, maybe you could include the MLE estimate and MLE fit spectra to
173 show the differences?

174 JN: Perhaps you might also include 2 spectra? One for low and one for high epsilon?

175 d. *flowspeed past the sensor*

176 The flowspeed past the thermistor is needed to convert the measured temperature derivative
177 dT/dt to a spatial gradient. For the CTD- χ pod, the largest contribution to the flowspeed is usu-
178 ally the vertical velocity of the CTD package (dp/dt), which is close to 1m/s on average, so we
179 typically neglect the horizontal component of velocity in converting from frequency to wavenum-
180 ber spectra.

181 JN: but isn't it the swell-induced heave that is what sets the flow speed? I wonder if you
182 could/should show a series of spectra from some depth range over which chi/epsilon is relatively
183 constant, and then show a small snippet of data over which u changes appreciably, so that you
184 can see the different wavenumber spectra (maybe segregated by u (20-50 cm/s, 50-100 cm/s,

185 ζ 100 cm/s)). I.e., you could show raw T, depth vs time, dT/dt , etc., so that you can see how
186 the data get contaminated, that you have to ignore the contaminated spectra, and then that the
187 non-contaminated parts are consistent, etc.

188 Although this will be a good approximation, errors may be introduced where horizontal veloci-
189 ties are large. Note that b Because it is the total instantaneous velocity magnitude that represents
190 flow past the sensor, neglecting the horizontal component of velocity (assuming $u=dp/dt$) means
191 we are always underestimating the true flowspeed past the sensor. When the CTD package is
192 equipped with LADCP, the true flowspeed can be measured. In some cases (including EQ14)
193 where the CTD was not equipped with LADCP, it would seem that the ship's ADCP could be
194 used to estimate the horizontal component of velocity. However, because the CTD does not travel
195 perfectly vertically in strong currents, this is difficult to do in practice. In a strong horizontal flow,
196 the CTD will drift with the current while descending, lowering the flow relative to the sensors.
197 On the upcasts, the CTD will be pulled against the current, increasing the flow relative to the sen-
198 sors. Since the CTD in EQ14 was not equipped with LADCP, we use dp/dt as the flowspeed, and
199 estimate potential errors in the appendix.

200 4. Oceanographic Setting and Conditions

201 Brief overview of dynamics in study region? More details are given in Warner et al (in prep).
202 JN - maybe you can omit this section, but add a few more details in section 2?

203 5. Results

204 a. Direct Test of χ pod Method

205 We begin by utilizing the highly-resolved turbulence profiler data (for which both ε and χ are
206 measured) to test the assumptions of equation in estimating χ 4 (e.g., how we compute n2, dt/dz,

assumption of krho=kt, etc. We first apply the χ pod method to each Chameleon profile, using only the FP07 thermistor data. These results, which we will refer to as χ_χ , are then compared with χ_ε , computed by integrating the temperature gradient spectrum with k_b computed directly from shear-probe derived ε . Qualitatively, χ_χ and χ_ε show very similar depth and time patterns (Figure 5), suggesting the method generally works well. A more quantitative comparison is made with a 2-D histogram (Figure 6), which shows that the two are well-correlated over a wide range of magnitudes.

214 b. CTD χ -pod - Chameleon Comparison

Having demonstrated that the method works for Chameleon data, we now compare χ from CTD-mounted χ pods to χ_ε . In contrast to the Chameleon data, the CTD is more strongly coupled to the ship, and therefore subject to more vibration, heaving, and artificial turbulence created by the rosette. A total of 38 CTD- χ pod casts were done with chameleon profiles immediately before and after. We first compare CTD- χ pod profiles to the mean of Chameleon profiles bracketing each cast, both averaged in 5m depth bins (Figure 8). The two appear to be correlated, with considerable scatter. However, we expect significant natural variability even between chameleon profiles. Scatter plots of before/after chameleon profiles (not shown), typically separated by about an hour, show a similar level of scatter as the differences between methods, suggesting that the observed differences (Figure 8) can be explained by natural variability in turbulence. This is demonstrated by histograms of the ratio of χ from adjacent casts (Figure 9) which show that the variability between CTD χ pod and chameleon casts is similar to the natural variability between before/after chameleon profiles. Average profiles from all CTD-chameleon pairs (Figure 10) overlap within 95% confidence limits at all depths where there exists good data for both. Averages of subsets of profiles clustered in position/time (not shown) also agree.

230 **6. Discussion**

231 We have shown that χ can be accurately estimated from χ pods attached to CTD rosettes.

232 *JN: I would consider going through each of the assumptions (maybe in bullets, to explain that
233 you test the effects of these (in the appendix, or elsewhere, and that they have small effect. include
234 gamma = 0.05, 0.1, 0.2, 0.4 and state explicitly the effect on χ . State the findings of n2, dtdz too..?*

235 One major assumption is the mixing efficiency Γ . A value of 0.2 is commonly assumed, but
236 evidence suggests this may vary significantly. The χ pod method also assumes that $K_T = K_\rho$. Even
237 if ε estimates have a large uncertainty, χ and K_T are robust and should be useful to the community.

238 *JN: Also make some summary statement of the amount of data thrown out because of swell con-
239 tamination, and make some statement about how you get the same answer regardless of instan-
240 taneous dp/dt. For example, you could segregate data, and compute χ for all profiles, including
241 only instantaneous $u < 0.5$, and $u > 1.0$, and show that the 100-m means of those are the same....
242 which means we're not getting contamination / bias from the variability in dp/dt?*

243 The goal of CTD- χ pods is to expand the number and spatial coverage of ocean mixing ob-
244 servations. We have already deployed instruments during several experiments (IWISE, TTIDE)
245 and on several GO-SHIP repeat-hydrography cruises. We plan to continue regular deployment on
246 GO-SHIP and similar cruises, adding χ and K_T to the suite of variables measured and enabling
247 scientists to explore relationships between these and other variables. The expanding database of
248 mixing measurements from CTD- χ pods will also enable testing of other commonly-used or new
249 mixing parameterizations. An example of data from a portion of the P16 GO-SHIP cruise is shown
250 in Figure 11.

251 **7. Conclusions**

252 Expand??

- The χ pod method was directly applied to temperature gradients measured by the chameleon microstructure profiler on 2742 profiles during the EQ14 cruises. The estimated χ_χ agrees well with χ_ε calculated using ε from shear probes over a wide range of magnitudes (Figure 6).
- CTD- χ pod profiles were also compared to nearby chameleon profiles during the cruise. Averaged profiles of χ agree within 95% confidence limits. No bias was detected between the estimates of χ .
- We conclude that estimates of χ and K_T from the CTD- χ pod platform are robust and reliable.

Acknowledgments. The EQ14 experiment was funded by ??. We thank the Captain and crew of R/V Oceanus. Also thank people who helped collect the data, those who made the sensors, etc..

APPENDIX A

Sensitivity to flowspeed

We investigate the sensitivity of the χ pod calculations to flowspeed, which is used to convert temperate gradient spectra from the frequency domain to the wavenumber domain via Taylor's frozen flow hypothesis. In this data, we have ignored any horizontal velocities and assumed the flow speed is equal to the vertical speed of the CTD rosette, determined from the recorded pressure dp/dt . To test the sensitivity of the χ pod method to flowspeed, we repeated the calculations with constant offsets added to the flowspeed. Since the total magnitude of velocity is used, dp/dt is a minimum estimate of the true speed. Adding 0.1(1)m/s results in a median error of 13(52) percent (Figure 12). Increasing the velocity tends to result in smaller values of χ , since it shifts the spectrum to lower wavenumbers.

APPENDIX B

Sensitivity to N^2 and dT/dz

276 We investigated the sensitivity of the calculations to N^2 , dT/dz . The iterative method to estimate
 277 chi requires the background stratification N^2 and temperature gradient dT/dz . We investigated the
 278 sensitivity of the results to the choice of scale over which these are computed or smoothed. The
 279 estimate of χ is insensitive to these scales. However, while dissipation rate ε and diffusivity K_T are
 280 more strongly affected because they are linearly related to these values. Computing N^2 and dT/dz
 281 over smaller scales results in larger values and hence some larger values of K_T .

APPENDIX C

Test of MLE fitting method

284 We tested the spectrum fitting method of Ruddick et al. (2000) and found that this method does
 285 not work well for the χ pod data, where only a small fraction of the spectrum is resolved. In
 286 particular, the MLE method underestimates χ at larger magnitudes (Figure 13).

APPENDIX D

Variability of thermistor transfer functions

289 Measuring the transfer function for each individual thermistor proved too expensive and time-
 290 consuming. We found that using only frequencies up to 7Hz (where the transfer function is equal
 291 to or very close to unity) gives good agreement, and avoids the issue of the unknown transfer
 292 functions.

293 JN - I suggest you add the figure that shows the transfer functions for 10-20 thermistors, and has
294 a little histogram that convinces the reader that $XX = 90 \pm YY\%$ of the variance is resolved if one
295 chooses 7 Hz, but if you go out to 15-20 Hz, there is a large variability.

296 **References**

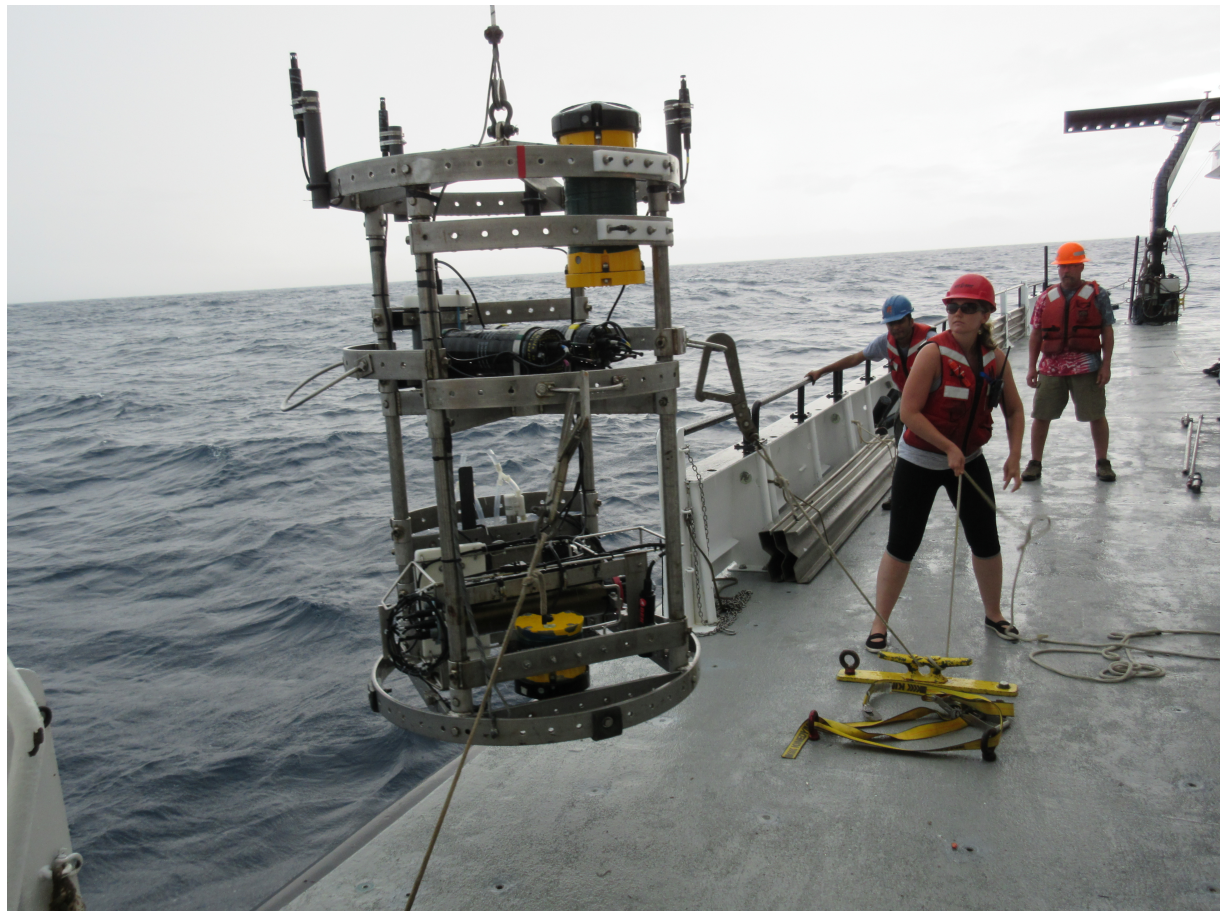
- 297 Alford, M., and R. Pinkel, 2000: Patterns of turbulent and double diffusive phenomena: Observa-
298 tions from a rapid profiling conductivity probe. *J. Phys. Oceanogr.*, **30**, 833–854.
- 299 Batchelor, G. K., 1959: Small-scale variation of convected quantitites like temperature in turbulent
300 fluid. *J. Fluid Mech.*, **5**, 113–139.
- 301 Dillon, T. M., 1982: Vertical overturns: A comparison of Thorpe and Ozmidov length scales. *J.*
302 *Geophys. Res.*, **87**, 9601–9613.
- 303 Galbraith, P. S., and D. E. Kelley, 1996: Identifying overturns in CTD profiles. *J. Atmos. Ocean.*
304 *Tech.*, **13**, 688–702.
- 305 Gregg, M., 1989: Scaling turbulent dissipation in the thermocline. *J. Geophys. Res.*, **94 (C7)**,
306 9686–9698.
- 307 Kunze, E., E. Firing, J. Hummon, T. K. Chereskin, and A. Thurnherr, 2006: Global abyssal mixing
308 inferred from lowered ADCP shear and CTD strain profiles. *Journal of Physical Oceanography*,
309 **36 (8)**, 1553–1576.
- 310 Mater, B. D., S. K. Venayagamoorthy, L. S. Laurent, and J. N. Moum, 2015: Biases in Thorpe scale
311 estimates of turbulence dissipation Part I: Assessments from large-scale overturns in oceano-
312 graphic data. *J. Phys. Oceanogr.*, **45 (2015)**, 2497–2521.

- 313 Melet, A., R. Hallberg, S. Legg, and K. L. Polzin, 2013: Sensitivity of the ocean state to the
314 vertical distribution of internal-tide-driven mixing. *J. Phys. Oceanogr.*, **43** (3), 602–615, doi:
315 <http://dx.doi.org/10.1175/JPO-D-12-055.1>.
- 316 Moum, J., and J. Nash, 2009: Mixing measurements on an equatorial ocean mooring. *J. Atmos.*
317 *Ocean. Tech.*, **26**, 317–336.
- 318 Munk, W., and C. Wunsch, 1998: Abyssal recipes II: energetics of tidal and wind mixing. *Deep-*
319 *Sea Res. Part I*, **45**, 1977–2010.
- 320 Munk, W. H., 1966: Abyssal recipes. *Deep-Sea Res.*, **13**, 707–730.
- 321 Osborn, T. R., 1980: Estimates of the local rate of vertical diffusion from dissipation measure-
322 ments. *J. Phys. Oceanogr.*, **10**, 83–89.
- 323 Osborn, T. R., and C. S. Cox, 1972: Oceanic fine structure. *Geophys. Fluid Dyn.*, **3**, 321–345.
- 324 Polzin, K. L., A. C. Naveira Garabato, T. N. Huussen, B. M. Sloyan, and S. N. Waterman, 2013:
325 Finescale parameterizations of turbulent dissipation. *Rev. Geophys.*, **submitted**.
- 326 Ruddick, B., A. Anis, and K. Thompson, 2000: Maximum likelihood spectral fitting: The Batch-
327 elor spectrum. *J. Atmos. Ocean. Tech.*, **17**, 1541–1555.
- 328 Scotti, A., 2015: Biases in Thorpe scale estimates of turbulence dissipation Part II: Energetics
329 arguments and turbulence simulations. *J. Phys. Oceanogr.*, **45** (2015), 2522–2543.
- 330 Thorpe, S., 1977: Turbulence and mixing in a Scottish Loch. *Philos. Trans. R. Soc. London Ser.*
331 *A*, **286**, 125–181.
- 332 Waterhouse, A. F., and Coauthors, 2014: Global patterns of diapycnal mixing from measurements
333 of the turbulent dissipation rate. *J. Phys. Oceanogr.*, **44** (7), 1854–1872.

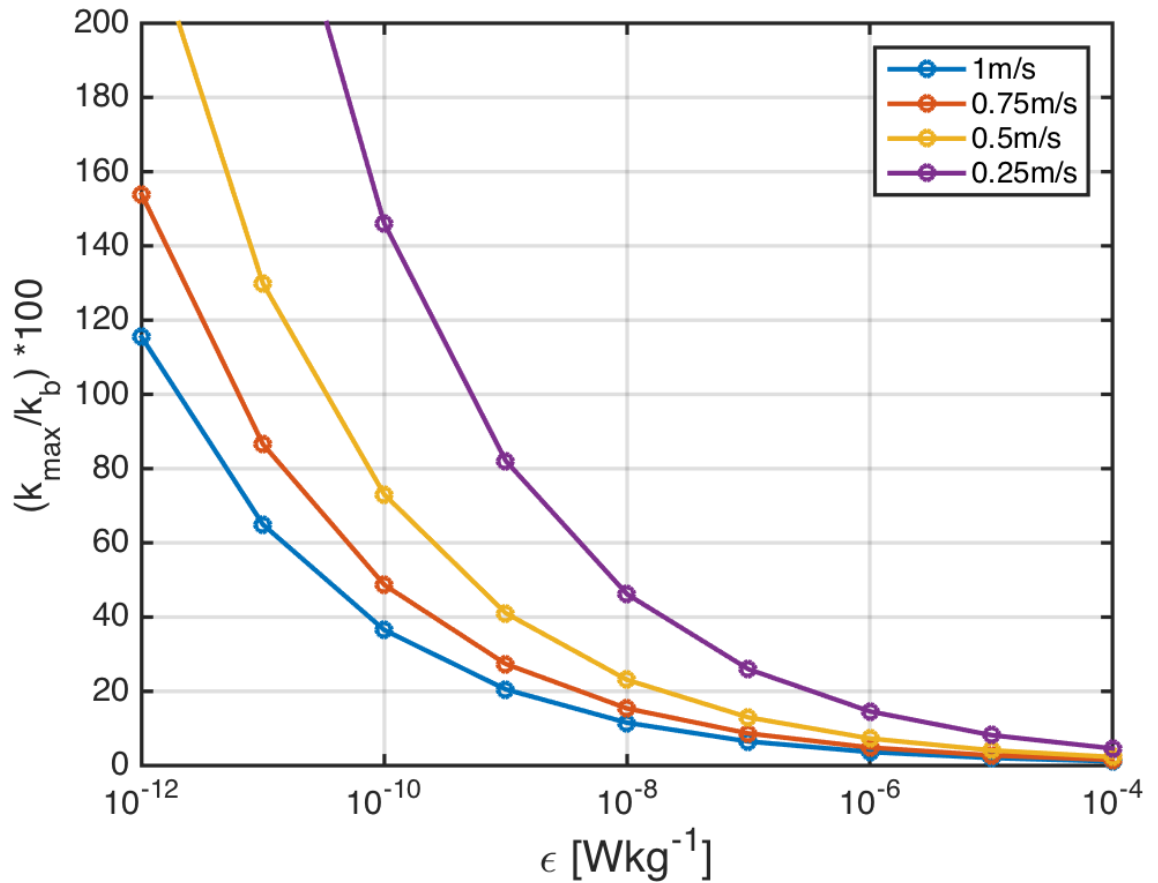
- 334 Waterman, S., A. C. N. Garabato, and K. L. Polzin, 2013: Internal waves and turbulence in the
335 antarctic circumpolar current. *Journal of Physical Oceanography*, **43** (2), 259–282.
- 336 Whalen, C. B., J. A. MacKinnon, L. D. Talley, and A. F. Waterhouse, 2015: Estimating the
337 mean diapycnal mixing using a finescale strain parameterization. *Journal of Physical Oceanog-
338 raphy*, **45** (4), 1174–1188, doi:10.1175/JPO-D-14-0167.1, URL [http://dx.doi.org/10.1175/
339 JPO-D-14-0167.1](http://dx.doi.org/10.1175/JPO-D-14-0167.1).
- 340 Whalen, C. B., L. D. Talley, and J. A. MacKinnon, 2012: Spatial and temporal variabil-
341 ity of global ocean mixing inferred from argo profiles. *Geophys. Res. Lett.*, **39** (L18612),
342 doi:10.1029/2012GL053196.

343 LIST OF FIGURES

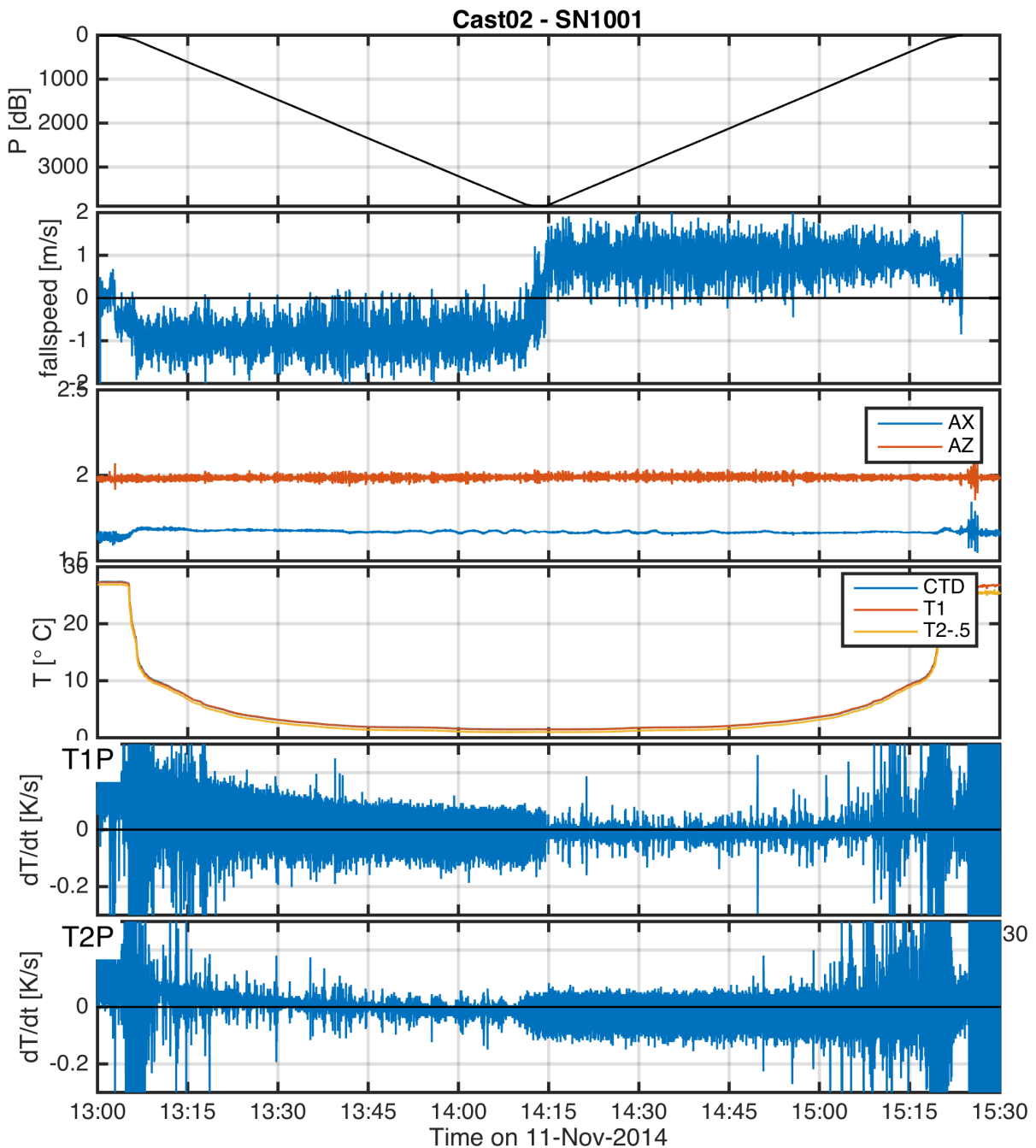
344	Fig. 1. Photo of CTD rosette during EQ14 with χ -pods attached. ** Add close-up picture of mini-	21
345	chipod unit too**	
346	Fig. 2. Ratio of the maximum observed wavenumber $k_{max} = f_{max}/fspeed$ to the Batchelor wavenum-	22
347	ber k_b for different values of ϵ , assuming a $f_{max} = 15Hz$. Each line is for a different	
348	flowspeed.	
349	Fig. 3. : add units / calibrate AX/AZ; also check to see if you've plotted dT/dt or $-dT/dt$. I think	23
350	it has the wrong sign/ I think that's what comes out of the electronics; also label T1P and	
351	T2P series "up-looking $dT1/dt$ " and "down-looking $dT2/dt$ " Example timeseries from one	
352	CTD cast during EQ14. a) CTD pressure. b) Fallspeed of CTD (dp/dt).c) Vertical and	
353	horizontal accelerations measured by χ -pod. d) Temperature from CTD and (calibrated) χ -pod	
354	sensors. T2 is offset slightly for visualization. e) Temperature derivative dT/dt measured	
355	by the upward-looking χ -pod sensor T1. f) Temperature derivative dT/dt measured by the	
356	downward-looking χ -pod sensor T2.	
357	Fig. 4. JN: why choose an example where epsilon and epsilon chi are so different? Can we find a	24
358	better one? Example temperature gradient spectra from EQ14. Solid black line show the	
359	observed spectra. Dashed magenta line shows the fit theoretical Kraichnan spectra for the	
360	χ pod estimates. Purple line is Kraichnan spectra for chameleon χ and ϵ . Vertical dashed	
361	blue lines indicate the minimum and maximum wavenumber used in the χ pod calculation.	
362	The Batchelor wavenumber k_b is also indicated by the cyan line.	
363	Fig. 5. Depth-time plots of $\log_{10}\chi$ from both methods for EQ14 data. Top: χ pod method. Black	25
364	diamonds indicate casts used for comparison with CTD- χ pod profiles. Bottom: Chameleon.	
365	Fig. 6. 2D histogram of $\log_{10}(\chi)$ from chameleon (x-axis) and χ pod method (y-axes). Values from	26
366	each profile were averaged in the same 5m depth bins.	
367	Fig. 7. Histogram of the (left) ratio of the maximum observed wavenumber k_{max} to the Batchelor	27
368	wavenumber k_b , and (right) $fspeed$ for all profiles in EQ14.	
369	Fig. 8. Scatter plot of χ from CTD- χ pod profiles versus the mean of bracketing chameleon profiles.	28
370	Black dashed line shows 1:1, red are $\pm 10\chi$. **replace with histogram of ratios, or combine	
371	into one figure?**	
372	Fig. 9. Histogram of \log_{10} of the ratio of χ for nearby casts. The first set is for the before	29
373	(cham1) and after (cham2) chameleon profiles. the 2nd is CTD- χ pod profiles versus the	
374	before(cham1) profiles. The last is CTD- χ pod profiles versus the after(cham2) profiles.	
375	Dashed lines show the medians of each set. Note that bias is small/zero, and the variability	
376	(spread) between CTD/cham is similar to the natural variability between cham profiles.	
377	Fig. 10. Time mean of χ for all CTD- χ pod - chameleon cast pairs, with 95% bootstrap confidence	30
378	intervals.	
379	Fig. 11. Example chipod data from P16N. Top: $dTdz$. Bottom: χ .	31
380	Fig. 12. Histogram of % error for χ computed with constant added to fallspeed, in order to examine	32
381	sensitivity to fallspeed.	



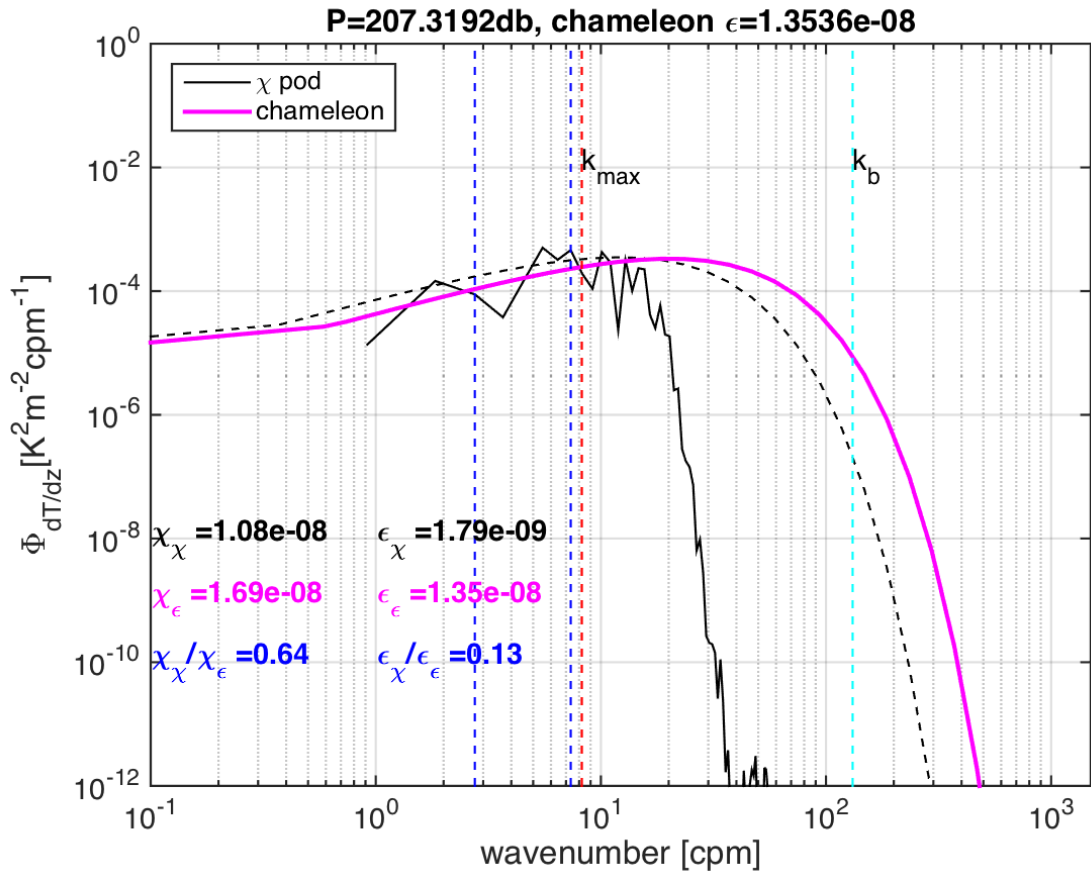
386 FIG. 1. Photo of CTD rosette during EQ14 with χ -pods attached. ** Add close-up picture of mini-chipod
387 unit too**



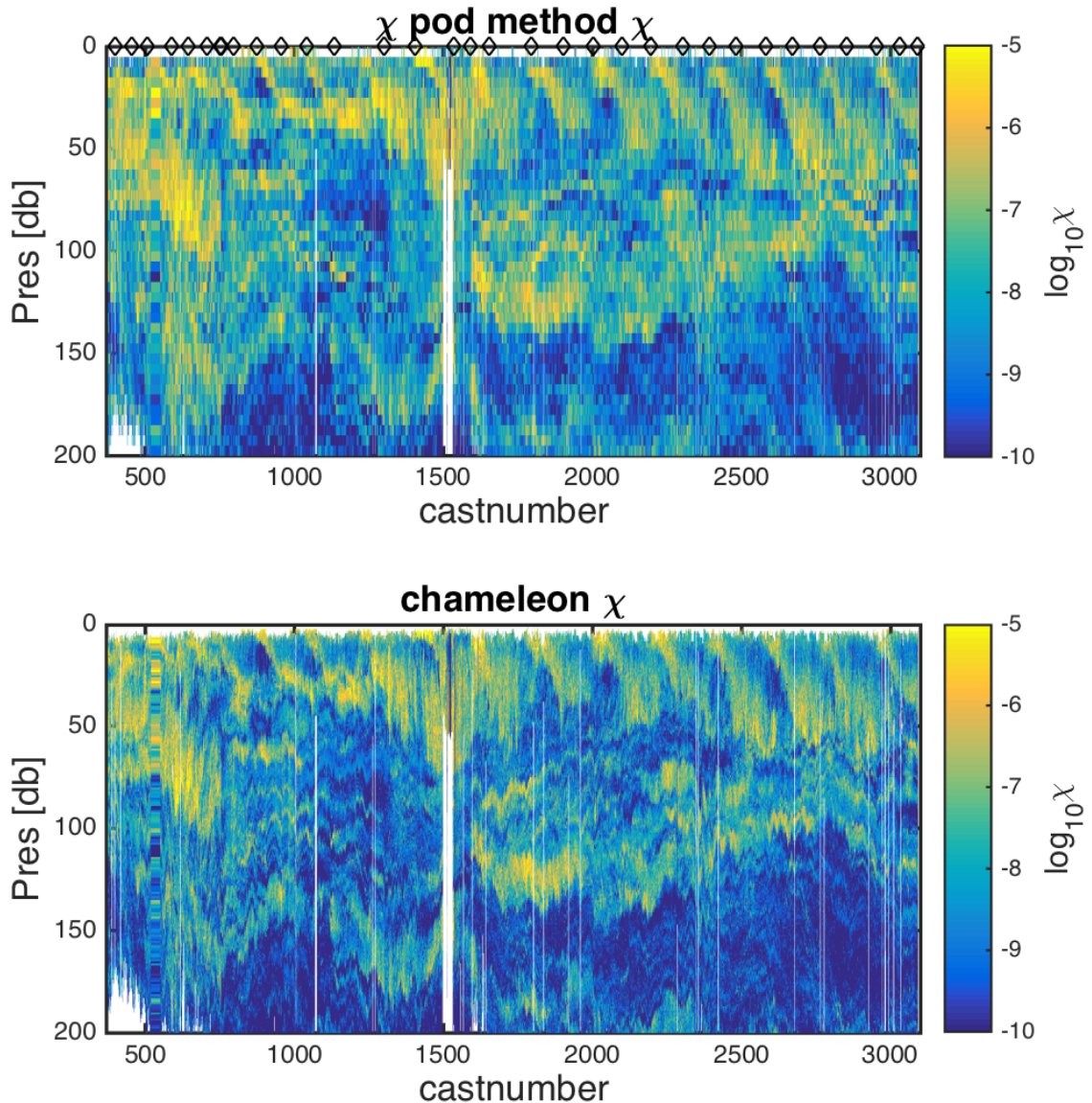
388 FIG. 2. Ratio of the maximum observed wavenumber $k_{\max} = f_{\max}/f_{spd}$ to the Bachelor wavenumber k_b for
 389 different values of ϵ , assuming a $f_{\max} = 15Hz$. Each line is for a different flowspeed.



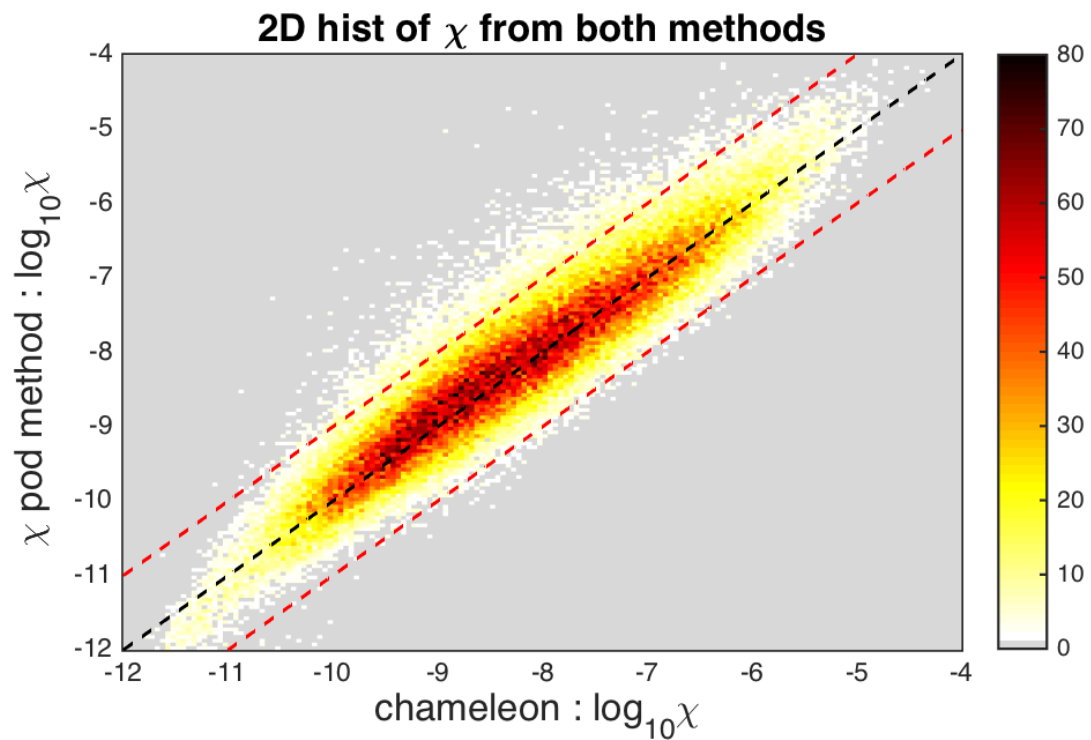
390 FIG. 3. : add units / calibrate AX/AZ; also check to see if you've plotted dT/dt or $-dT/dt$. I think it has the
 391 wrong sign/ I think that's what comes out of the electronics; also label T1P and T2P series "up-looking dT_1/dt "
 392 and "down-looking dT_2/dt " Example timeseries from one CTD cast during EQ14. a) CTD pressure. b) Fallspeed
 393 of CTD (dp/dt). c) Vertical and horizontal accelerations measured by χ -pod. d) Temperature from CTD and
 394 (calibrated) χ -pod sensors. T2 is offset slightly for visualization. e) Temperature derivative dT/dt measured
 395 by the upward-looking χ -pod sensor T1. f) Temperature derivative dT/dt measured by the downward-looking



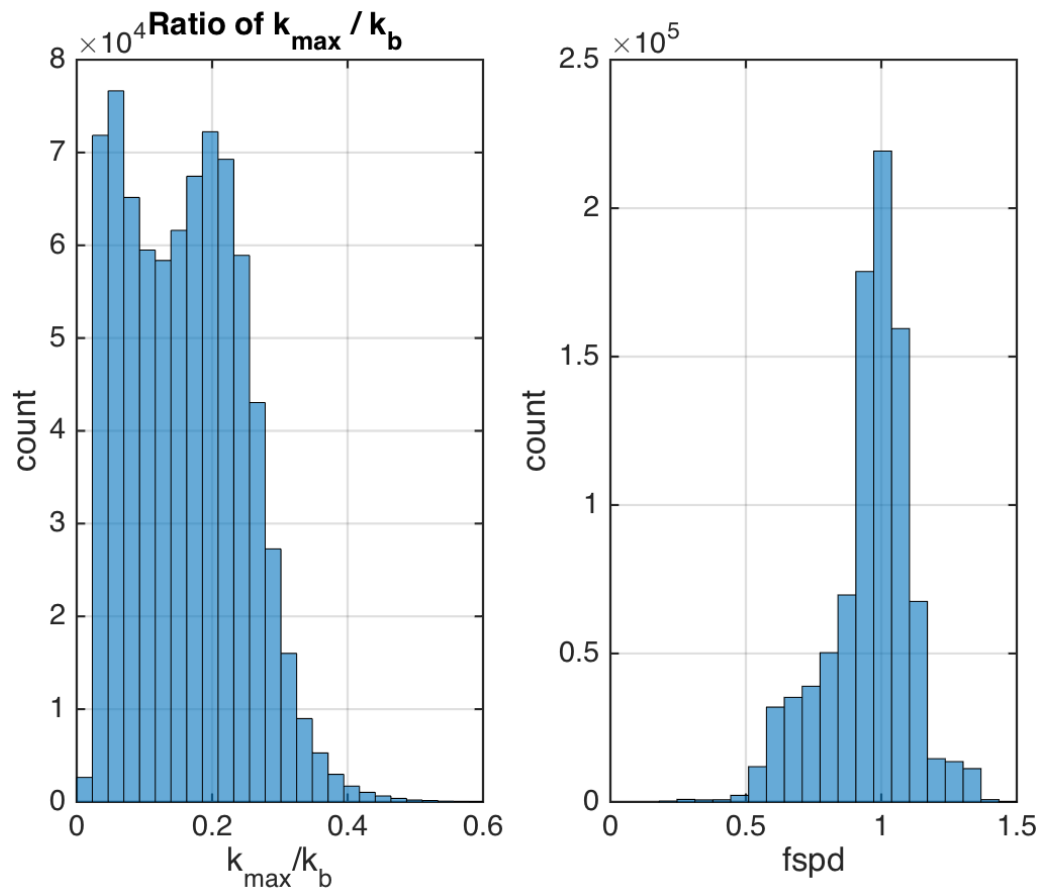
397 FIG. 4. JN: why choose an example where epsilon and epsilon chi are so different? Can we find a better
 398 one? Example temperature gradient spectra from EQ14. Solid black line show the observed spectra. Dashed
 399 magenta line shows the fit theoretical Kraichnan spectra for the χ pod estimates. Purple line is Kraichnan spectra
 400 for chameleon χ and ϵ . Vertical dashed blue lines indicate the minimum and maximum wavenumber used in the
 401 χ pod calculation. The Batchelor wavenumber k_b is also indicated by the cyan line.



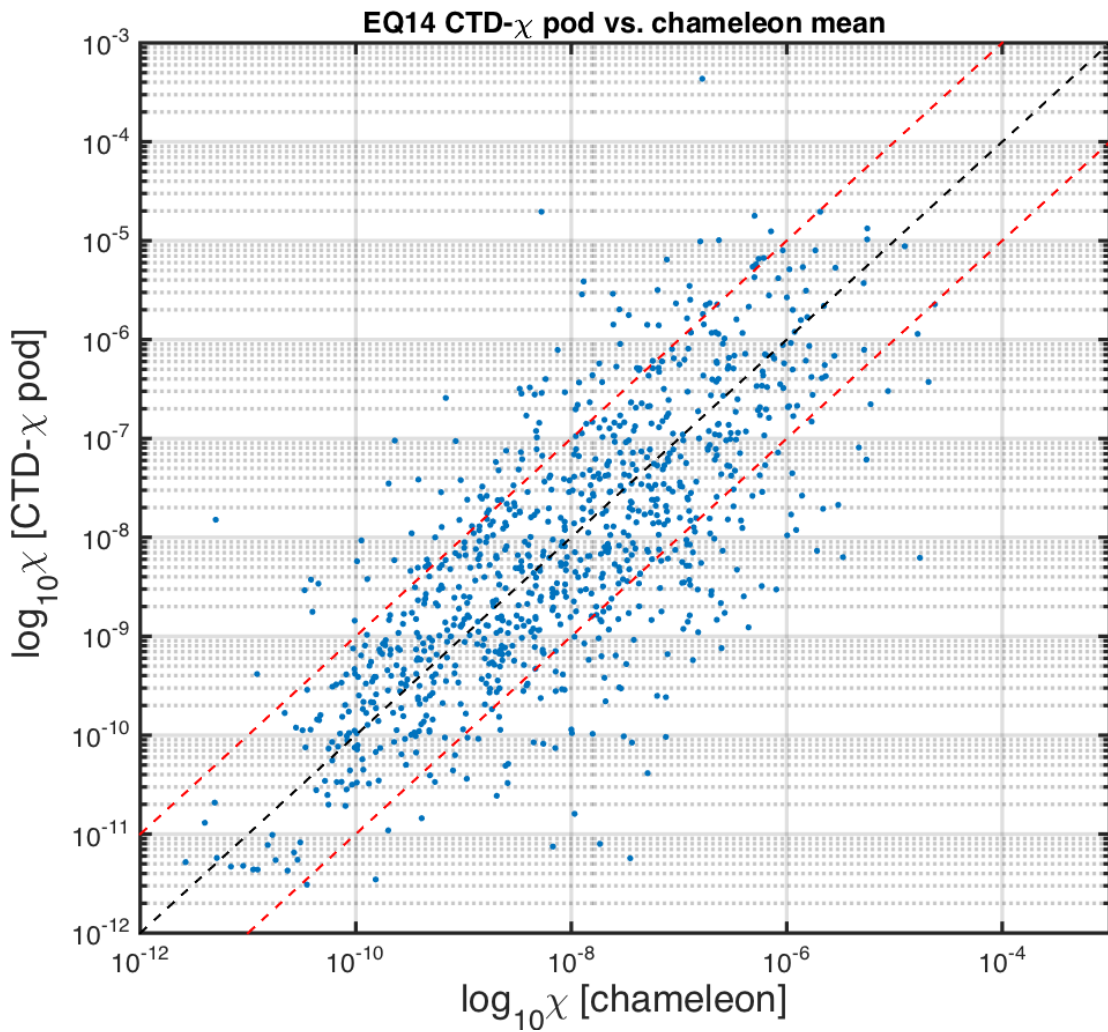
402 FIG. 5. Depth-time plots of $\log_{10} \chi$ from both methods for EQ14 data. Top: χ pod method. Black diamonds
 403 indicate casts used for comparison with CTD- χ pod profiles. Bottom: Chameleon.



⁴⁰⁴ FIG. 6. 2D histogram of $\log_{10}(\chi)$ from chameleon (x-axis) and χ_{pod} method (y-axes). Values from each
⁴⁰⁵ profile were averaged in the same 5m depth bins.



406 FIG. 7. Histogram of the (left) ratio of the maximum observed wavenumber k_{max} to the Bachelor wavenumber
 407 k_b , and (right) fspd for all profiles in EQ14.



⁴⁰⁸ FIG. 8. Scatter plot of χ from CTD- χ pod profiles versus the mean of bracketing chameleon profiles. Black
⁴⁰⁹ dashed line shows 1:1, red are $\pm 10 \times$. **replace with histogram of ratios, or combine into one figure?**

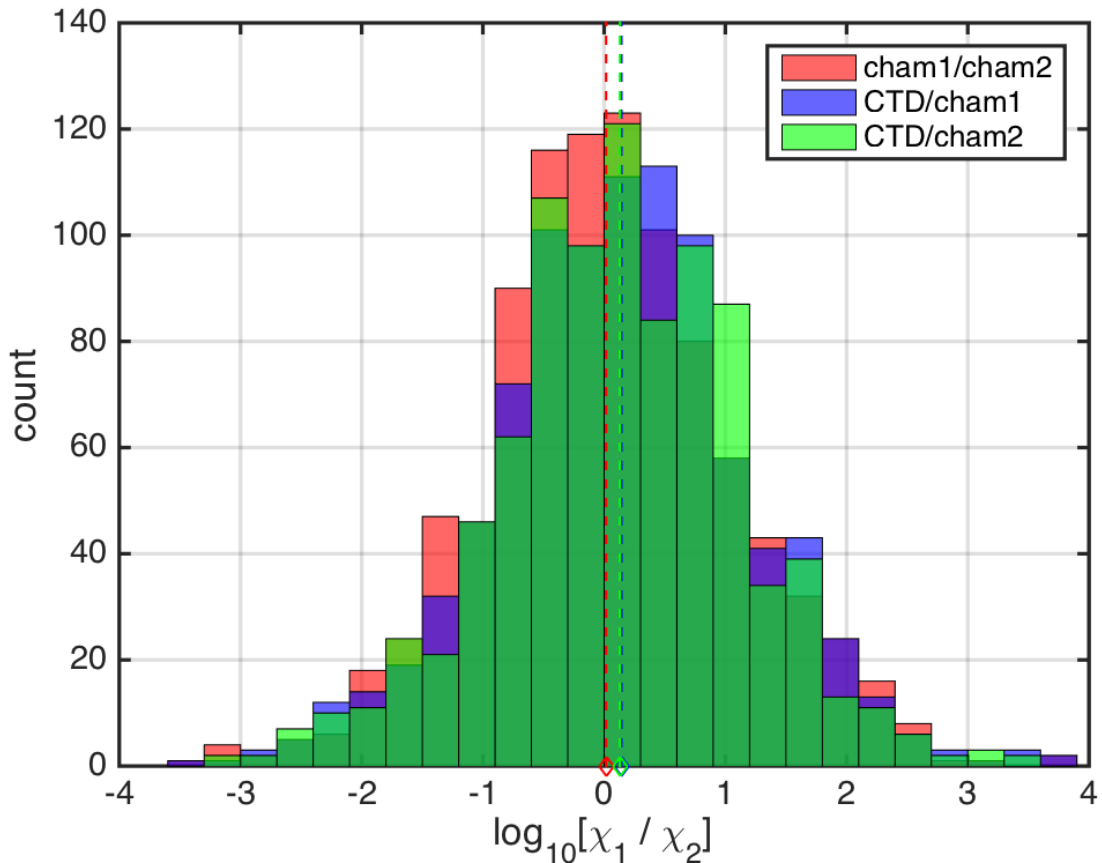


FIG. 9. Histogram of \log_{10} of the ratio of χ for nearby casts. The first set is for the before (cham1) and after (cham2) chameleon profiles. the 2nd is CTD- χ pod profiles versus the before(cham1) profiles. The last is CTD- χ pod profiles versus the after(cham2) profiles. Dashed lines show the medians of each set. Note that bias is small/zero, and the variability (spread) between CTD/cham is similar to the natural variability between cham profiles.

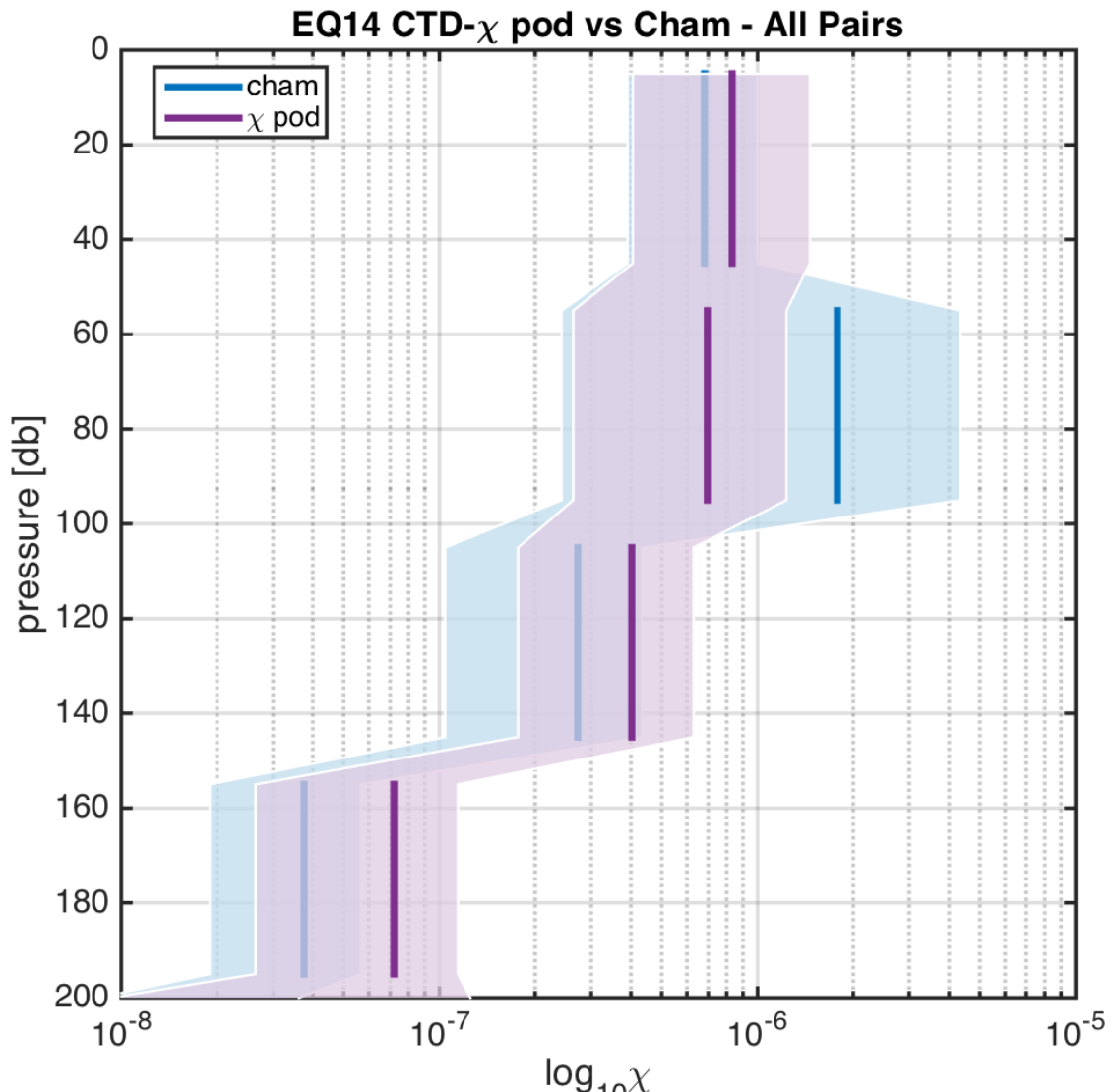


FIG. 10. Time mean of χ for all CTD- χ pod - chameleon cast pairs, with 95% bootstrap confidence intervals.

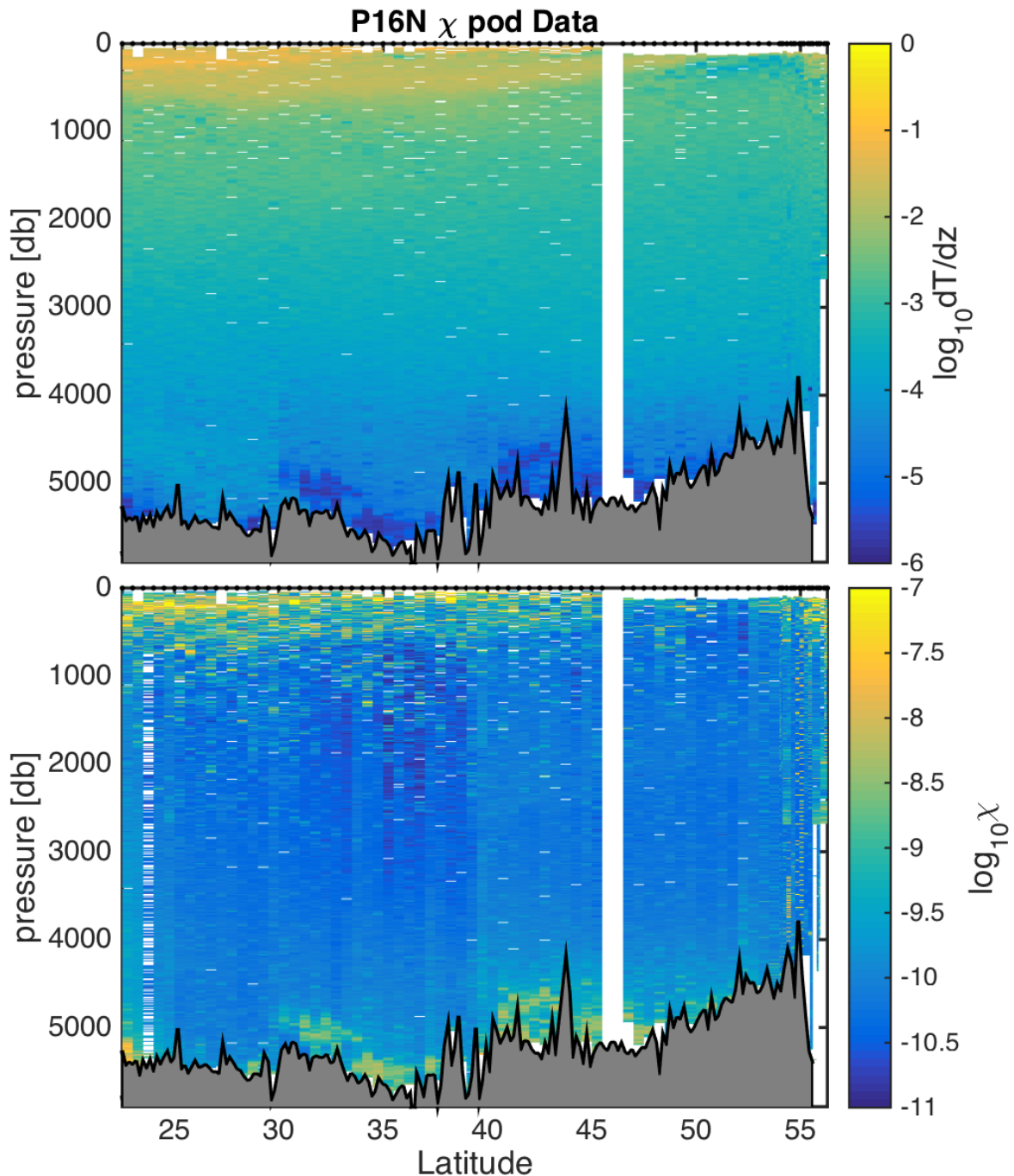
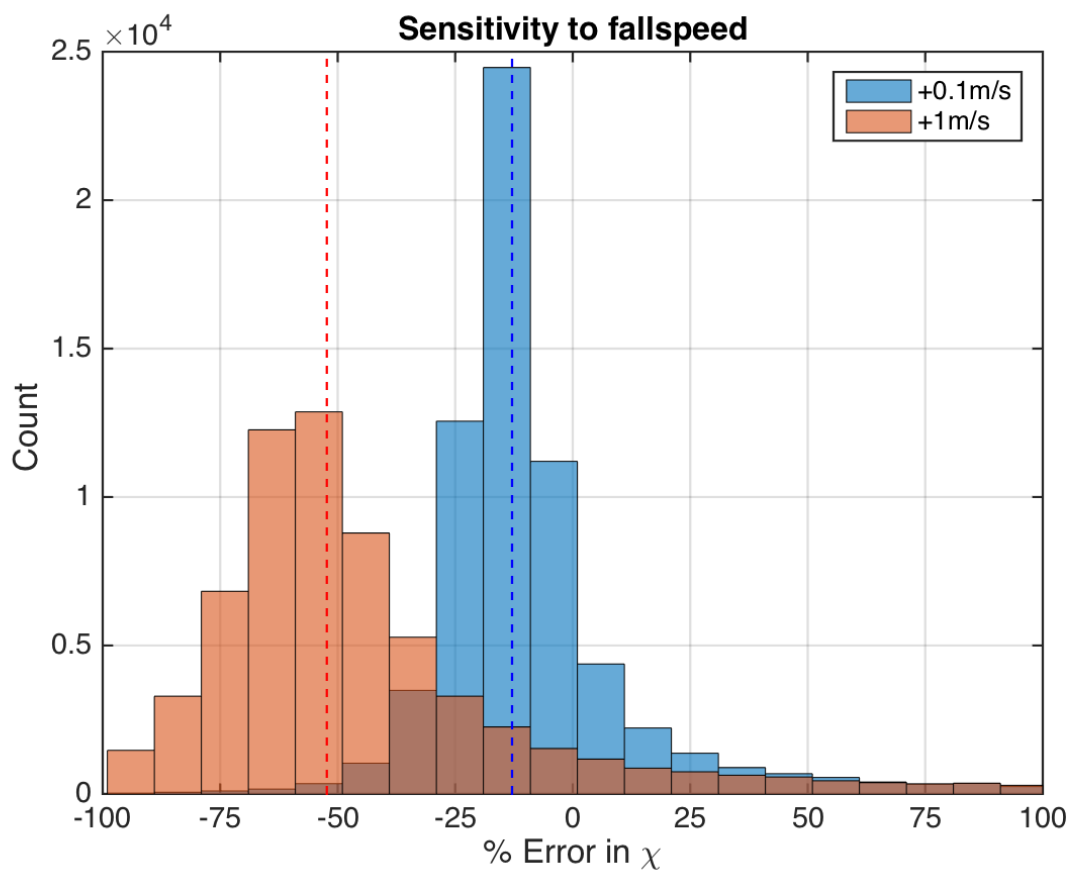
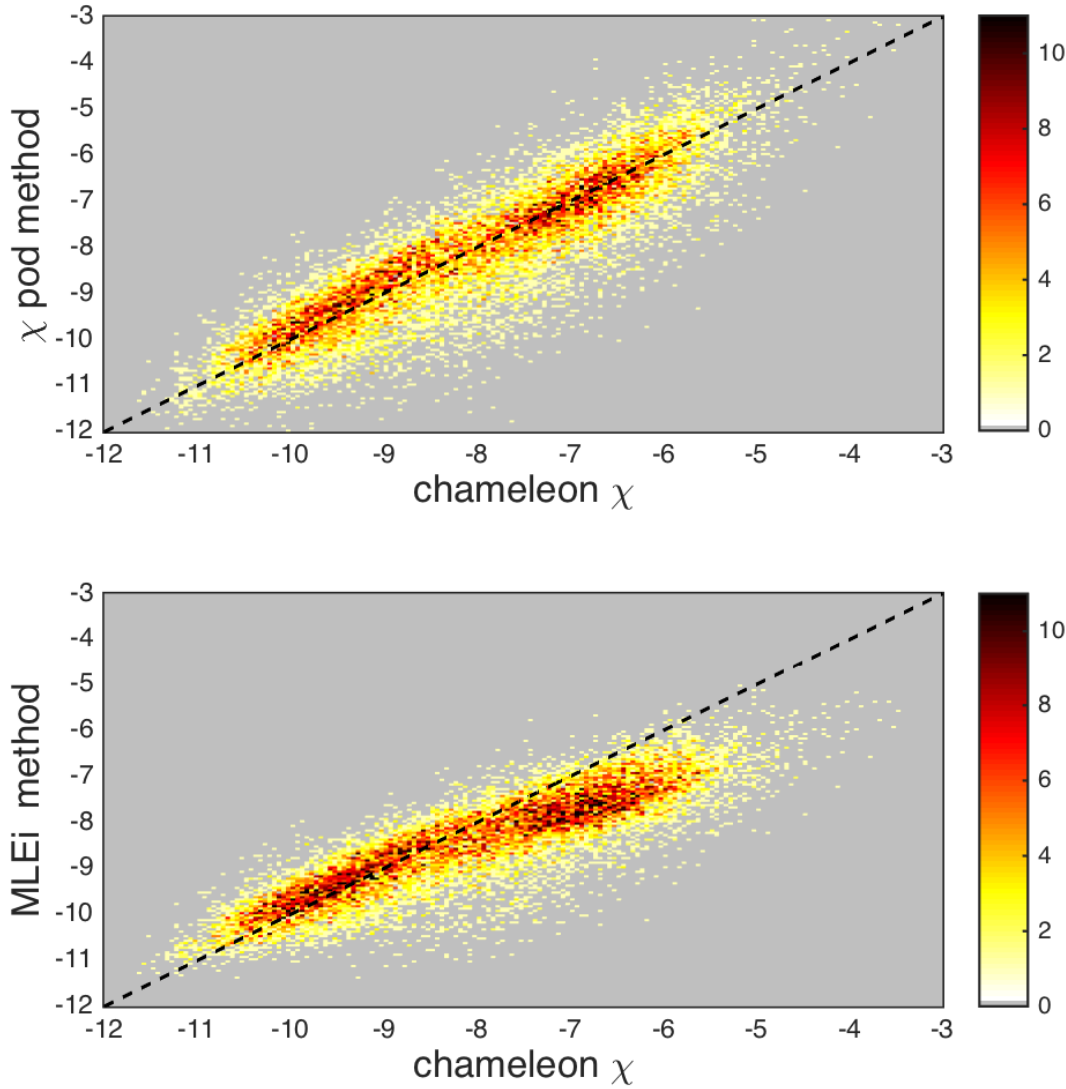


FIG. 11. Example chipod data from P16N. Top: $dTdz$. Bottom: χ .



415 FIG. 12. Histogram of % error for χ computed with constant added to fallspeed, in order to examine sensitivity
 416 to fallspeed.



417 FIG. 13. 2D histograms of χ computed using the iterative χ -pod method (top; equation XX) and the MLE fit
 418 (bottom; equation YY) versus χ computed from Chameleon for EQ14 CTD-chipod casts. *JN - are you really*
 419 *using the CTD chipod casts and not the Chameleon casts?* Note that the MLE method underestimates χ at larger
 420 magnitudes.